Biomass and Bioenergy 204 (2026) 108385

Contents lists available at ScienceDirect

Biomass and Bioenergy

journal homepage: www.elsevier.com/locate/biombioe

Development and optimization of sustainable activated biochar from waste pigeon pea stalks for efficient adsorptive removal of methylene blue from water

Shubhangi Umare [a], Ajay K. Thawait [a], Sumit H. Dhawane [b,*]

[a] Department of Civil Engineering, Maulana Azad National Institute of Technology, Bhopal, 462003, India
[b] Department of Chemical Engineering, Maulana Azad National Institute of Technology, Bhopal, 462003, India

ARTICLE INFO

Keywords:
Activated biochar
Waste agricultural residue
Pigeon pea stalk
Taguchi method
Optimization

ABSTRACT

This study explores the valorization of pigeon pea stalk waste (PPSW) through the synthesis of activated biochar (AB) with enhanced adsorption properties for the efficient removal of methylene blue (MB) from aqueous solutions. Addressing both agricultural waste disposal and water pollution, the research converts PPSW into high value adsorbents. Two types of AB were synthesized using sodium hydroxide (NaOH) and zinc chloride ($ZnCl_2$) as activating agents, designated as NaOH/AB and $ZnCl_2$/AB, respectively. The synthesis process was optimized using an L9 orthogonal array design, evaluating four key parameters: activation temperature, activation time, reagent to carbon ratio, and stirring speed. The influence of these parameters on the adsorption capacity (AC) and removal efficiency (RE) of MB was further examined through parametric studies. Statistical optimization and analysis were performed using ANOVA to validate the significance of each factor. The synthesized ABs were characterized using advanced analytical techniques. For NaOH/AB, optimal conditions yielding 100 % RE were found to be an activation temperature of 40 °C, activation time of 12 h, reagent-to-carbon ratio of 2:1, and stirring speed of 400 rpm. In the case of $ZnCl_2$/AB, maximum AC of 7.51 mg/g and 100 % RE were achieved at 80 °C, 12 h, a 6:1 reagent-to-carbon ratio, and 600 rpm stirring speed. The results confirm that AB derived from PPSW using NaOH and $ZnCl_2$ exhibits excellent adsorption performance and is highly effective in the complete removal of MB from contaminated water.

1. Introduction

Rapid urbanization, industrialization, and intensive agricultural practices generate vast quantities of agricultural, industrial, food, forest, and other types of waste [1]. While a small portion of agricultural and forest residues is utilized for purposes such as animal grazing, manure preparation, and biogas production, a substantial amount is still either burned or dumped in landfills, contributing significantly to environmental pollution. India alone produces nearly 500 million metric tonnes of agricultural waste annually [2]. Improper waste disposal has led to the contamination of soil, water, and air, posing serious threats to ecological balance and human health. Over time, this environmental degradation could have far reaching consequences for the country food and nutritional security [2].

The current utilization of agricultural waste in India reflects limited value addition and incomplete resource recovery. The distribution of agricultural waste usage is approximately as follows: 29 % for animal feed, 23 % for domestic cooking fuel, 18 % for thatching and farm equipment, 12 % for industrial applications such as paper and board manufacturing, while the remaining 18 % is either left unutilized or burned in fields [3]. However, these conventional methods face several challenges, including low economic returns, seasonal availability, transportation difficulties, and insufficient processing infrastructure [4].

Industrial applications of agricultural waste currently focus on pulp and paper production (utilizing 15–20 % of total waste), construction materials (5–8 %), and bioenergy generation (3–5 %). Despite these applications, the majority of agricultural residues remain underutilized due to technological gaps, lack of value addition processes, and insufficient market linkages. Recent technological developments have identified the potential for converting agricultural waste into high value products, including activated carbon, biochar, biofuels, and biochemicals, which can achieve economic returns 3–5 times higher than

* Corresponding author. Department of Chemical Engineering, MANIT, Bhopal, India.
E-mail addresses: sumitdhawane@manit.ac.in, sdhawane17@gmail.com (S.H. Dhawane).

https://doi.org/10.1016/j.biombioe.2025.108385
Received 20 January 2025; Received in revised form 3 September 2025; Accepted 10 September 2025
Available online 23 September 2025

those of conventional uses [5]. However, the challenge lies in developing cost effective conversion technologies that can be implemented at decentralised scales, enabling rural communities to access higher value markets while addressing environmental concerns associated with open-burning practices [3].

Biochar is a fine material obtained from biomass available in the environment [6]. It is also known as AB or activated carbon after the modification of raw biochar with a physicochemical activation. Biochar is highly porous and has a higher specific surface area and catalytic properties than raw biochar [7]. The different biomass properties such as moisture content, ash content, volatile matter, fixed carbon, cellulose, hemicellulose and lignin content significantly affect its derived biochar features. However, applying biochar can solve various environmental problems, which helps to mitigate a demolished ecosystem. AB synthesis comprises the conversion of raw biomass into active products, mainly through thermochemical and biochemical conversion. The most common methods used for thermochemical conversion are pyrolysis and gasification. Likewise, fermentation and anaerobic incorporation are used in the biochemical conversion. Pyrolysis is a thermochemical process without an oxygen atmosphere (300°C–900 °C) that converts raw biomass into valuable goods in solid, liquid, and gaseous forms. Similarly, AB can be prepared by two activation methods: physical activation (nitrogen, air, steam, etc.) and chemical activation (NaOH, KOH, H_2SO_4, HNO_3) to improve the surface area, porosity and functional groups [8]. The pyrolysis mechanism of PPSW for recognizing the biopolymeric changes of each constituent, and discovering the stage change locations for shifting the degradation zone from one polymer to another has been studied [9]. Another study carried out for focusing on pyrolysis heating temperatures and the characterization of pigeon pea stalks [10]. Likewise, Kirti et al. studied kinetic parameters parallel with the thermodynamic investigation and reaction methods pertaining to the pyrolysis of PPSW [11]. Further, Torrefaction on physicochemical features of pigeon pea stalks was studied [12].

Several agricultural crop residues, like rice husk [13], rice straw [14], wheat straw [15], sugarcane bagasse [16], cotton stalk [17], maize stalk [18], coconut shell [19], sorghum stalk [20], pearl millet stalk [21], palm shell [22], almond shell [23], coconut husk [24], olive husk [25], coffee husk [26], Peanut husk [27], bamboo waste [28], mustard stalk [29], chickpea stalk [30], Jute fiber [31], crops stems, leaves, and seeds were investigated for their potential capacity to produce biochar. Amongst multiple agricultural crop residues, pigeon pea is a type of pulse widely cultivated throughout the globe, including India. It is commonly known as 'Tur' or 'Arhur' in rural areas of India. Overall, India ranks 1st in the production of pigeon peas, sharing 78.87 % (FAO, 2021) of global production. The leading producers of the pigeon pea crop in India are the states of Maharashtra, Uttar Pradesh, Karnataka, Madhya Pradesh, and Gujarat. Pigeon pea crops yield almost 2.9 (tons/ha) stalk waste, which is considerably more than other agricultural crop like peanut stalk (2.6 tons/ha), mustard stalk (1.9 tons/ha), chickpea stalk (0.9 tons/ha), pearl millet stalk (1.3 tons/ha), and sorghum stalk (1.6 tons/ha). PPSW is a primary woody waste residue obtained from pigeon pea crops [11]. In rural parts of India, PPSW is commonly used as a domestic fuel for cooking purposes. These biomass products could make biochar to reduce GHG emissions from open burning and improper utilization trends, thereby maximizing their potential capacity [32].

PPSW is an agricultural waste generated on farms, which should be converted into a valuable material such as biochar in an economical and sustainable manner. Therefore, optimizing the synthesis process and identifying the dominant parameters affecting biochar yield, AC, and RE is crucial. Optimization of such chemical activation processes can be carried out using various statistical techniques such as Response Surface Methodology (RSM), Central Composite Design (CCD), Box-Behnken Design (BBD), and the Taguchi method. Furthermore, the optimized AB was utilized for the removal of MB dye from water. Several studies have reported the removal of MB dye from water using various biomass derived adsorbents. For example, phosphoric acid (H_3PO_4) activated papaya peels were used to remove MB from aqueous solutions, achieving RE of 76.5 % at pH 2 and 92.67 % at pH 6 [33]. In another study, areca nut husk (AH) biomass was utilized to produce graphene oxide, which exhibited a RE of 93.05 % under optimal conditions: an initial dye concentration of 20 mg/L, an adsorbent dose of 0.5 g, and a contact time of 180 min [34]. Similarly, biomass derived from rubber seed pericarp was converted into highly porous activated carbon using H_3PO_4 as the activating agent. This activated carbon achieved 92 % MB removal under optimal conditions, including an initial concentration of 100 mg/L, pH 7.8, and an adsorbent dose of 0.05 g [35]. Another investigation employed torrefied biomass obtained from grape pomace for MB dye removal, achieving approximately 96.5 % removal under varied experimental conditions [36].

Most existing studies on biochar based adsorbents primarily emphasize on RE, often overlooking critical aspects such as optimization of synthesis parameters through statistical and computational modeling, cost analysis, and scalability assessment. Limited work exists on utilizing agricultural residues like PPSW for producing AB using dual activation strategies (alkali and Lewis acid), while benchmarking its performance against conventional adsorbents. This study addresses these gaps by optimizing activation conditions through advanced statistical techniques, achieving 100 % MB removal and incorporating economic analysis to ensure sustainability and large scale applicability.

Optimization plays a crucial role in minimizing resource consumption while maximizing performance. Among available techniques, the Taguchi method is highly effective as it reduces the experimental runs while identifying dominant factors influencing process outcomes. For AB synthesis, multiple process parameters significantly impact AC and RE, necessitating systematic evaluation. Moreover, the choice of activating agents strongly affects production cost and adsorbent characteristics. Hence, identifying optimal conditions for producing high-performance AB from PPSW is essential for developing an economical and sustainable solution for wastewater treatment.

Despite increasing interest in biochar, the use of PPSW as a feedstock for AB synthesis remains largely unexplored. Literature reveals a clear lack of comprehensive studies focusing on parameter optimization for PPSW derived biochar targeting MB adsorption. To fill this research gap, the present work synthesizes AB from PPSW using NaOH (a strong alkali) and $ZnCl_2$ (a Lewis acid) as activating agents, enabling comparative evaluation under extreme conditions. The activation process is optimized using the L9 orthogonal array design of the Taguchi method to identify key factors affecting structural and functional properties. This approach facilitates the development of a cost-effective and environmentally sustainable adsorbent with superior performance.

Beyond technical innovation, the current study contributes to circular bioeconomy development by valorizing agricultural residues, reducing greenhouse gas emissions from crop residue burning, and creating value added products that enhance rural economic resilience. The optimized AB not only demonstrates excellent adsorption capability for MB but also establishes a scalable methodology supported by process economics. Thus, this study advances sustainable wastewater treatment solutions by integrating material optimization, economic feasibility, and environmental impact assessment into a single framework.

2. Materials and methods

2.1. Materials

The agricultural biomass of PPSW was used as feedstock to prepare AB collected from the agricultural farm of Gadchiroli district, Maharashtra, India. Chemicals like sodium hydroxide (NaOH-98 %), zinc chloride ($ZnCl_2$-97 %), sulphuric acid (H_2SO_4- 98 %) and hydrochloric acid (HCL- 35.4 %) were bought from Pallav Chemicals Pvt. Ltd, India and MB dye ($C_{16}H_{18}N_3SCI$-99 %) was obtained from Sisco Research Laboratories Pvt. Ltd, India. Distilled water used in the study was

obtained from the Direct-Q water purification system (99.99 %), Germany.

2.2. Synthesis of AB

PPSW collected from agricultural farms was thoroughly washed twice with tap water to remove dust and impurities, followed by a rinse with distilled water. The cleaned biomass was first sun dried for 2–3 days and then oven dried at 120 °C for 24 h to ensure complete moisture removal. The dried stalks were cut into smaller pieces using a mechanical cutter to reduce their size for further processing.

The prepared biomass was carbonized in a tube furnace under a nitrogen atmosphere at 550 °C for 2 h. This carbonization temperature was selected based on a literature review on PPSW [11]. The resulting biochar was then chemically activated using NaOH and $ZnCl_2$ separately to enhance its surface characteristics. Optimization of the activation process was performed considering key parameters such as activation temperature, activation time, reagent to carbon ratio, and agitation speed, as outlined in Table 1. For each experimental set, AC and RE were measured and recorded as responses to the design of experiments.

After the activation period, the AB was washed repeatedly with distilled water until a neutral pH was achieved. The neutralized mixture was stirred for an additional 45 min and then filtered using Whatman filter paper. The resulting wet material was oven dried at 110 °C for 24 h, followed by calcination at 500 °C for 1 h. The calcined product was ground into a fine powder and designated as AB. The same procedure was repeated for the $ZnCl_2$-AB.

The adsorption performance of the synthesized AB was evaluated for MB removal from water, as shown in Table 1. A 100 ppm stock solution of MB was prepared by dissolving 0.01 g of MB in 100 mL of distilled water. A UV–Visible spectrophotometer (LABMAN, India) was used to measure MB concentration before and after adsorption at a wavelength of 664 nm. Batch adsorption experiments were conducted using 100 mL conical flasks, each containing 30 mL of MB solution (50 ppm) and 0.2 g of AB under the optimized conditions specified in Table 1 for both activating agents. The flasks were agitated at 250 rpm using a magnetic stirrer at room temperature for 2 h.

The AC (q_e) and removal efficacy (RE) of AB were determined using the given equation.

$$AC\ (mg/g) = \frac{Ci - Ce}{m} * V \quad (1)$$

$$RE\ (\%) = \frac{Ci - Ce}{Ci} * 100 \quad (2)$$

where, Ci (mg) is the initial concentration of a sample.
Ce (mg) is the final concentration of a sample.
V (L) is the Volume of the solution
m (g) is the weight of the adsorbent dose.

2.3. Design of experiments using L9 orthogonal array approach

The key factors influencing chemical activation include activation temperature, activation time, reagent to carbon ratio, and stirring speed. It is essential to evaluate the effect of each parameter and identify the optimal conditions to enhance the performance of AB. The Taguchi method is widely used in engineering and scientific research to address complex industrial optimization problems [8]. Unlike traditional approaches, which vary one parameter at a time while keeping others constant leading to increased experimental cost. The Taguchi method analyzes multiple parameters simultaneously, optimizing both the mean and variance of the response. This statistical technique enables determination of optimal conditions with a minimal number of experimental runs [33]. In this study, the L9 orthogonal array design under the Taguchi framework was employed to construct the experimental matrix, considering four parameters at three levels each, as shown in Table 2. The design was generated using Design Expert 13.0 software (STAT-EASE, USA). The required number of experimental runs was estimated using Equation (3).

$$N = (L - 1)\ P + 1 \quad (3)$$

where N is the number of experimental runs.
P is the number of parameters.
L is the Level.

2.4. Characterization of AB

The characterization of raw biochar, NaOH-AB and $ZnCl_2$-AB has been conducted separately. All ABs were primarily exposed to surface morphology using FESEM (EVO-18, Germany) to detect the pore formation on the surface of biochar. Similarly, EDX (Carle Zeiss Microscopy, Oxford-80, Germany) analysis was performed to investigate the elemental composition of AB. Likewise, the XRD (Brucker D2 Phaser Bench top XRD) of AB was conducted to determine the existence of a crystalline or amorphous structure on the surface of biochar. Furthermore, FTIR (IRAffinity-1S, Shimadzu, Japan) and Raman spectroscopy (IndiRam CTR-300) examinations of the NaOH/$ZnCl_2$-AB were conducted to determine the presence of functional and structural groups on the surface of AB.

Table 2
Selected parameters at three varied levels for L9 design matrix.

Factor	Parameters	Levels		
		1	2	3
A	Activation temperature (°C)	40	60	80
B	Activation time (h)	12	18	24
C	Reagent to carbon ratio	2:1	4:1	6:1
D	Stirring speed (RPM)	400	600	800

Table 1
Experimental designed matrix followed by Taguchi method with AC and RE.

Run	Activation Temperature (°C)	Activation Time (h)	Reagent to biochar ratio	Stirring speed (RPM)	AC (mg/g) NaOH/AB	RE (%)	AC (mg/g) $ZnCl_2$/AB	RE (%)
1	80	24	4:1	400	7.48	99.80	7.47	99.72
2	40	24	6:1	800	7.38	98.50	7.47	99.60
3	60	12	4:1	800	7.48	99.86	7.38	98.42
4	40	12	2:1	400	7.49	99.90	7.45	99.42
5	80	12	6:1	600	7.33	97.78	7.49	99.90
6	60	24	2:1	600	7.49	99.92	7.38	98.50
7	60	18	6:1	400	7.09	94.66	7.48	99.84
8	80	18	2:1	800	7.39	98.60	7.48	99.60
9	40	18	4:1	600	7.45	99.40	7.47	99.64

2.5. Adsorption kinetics

The adsorption kinetics, which determine the rate at which adsorbents remove MB dye, indicate the time required to reach equilibrium. In this study, the adsorption of MB dye onto NaOH-AB and $ZnCl_2$-AB was evaluated using pseudo-first-order and pseudo-second-order kinetic models, as expressed in equations (4) and (5) [34]. These models were chosen to clarify the adsorption mechanism: the pseudo-first-order model generally corresponds to physisorption involving weak van der Waals forces, whereas the pseudo-second-order model suggests chemisorption driven by electron sharing or exchange between adsorbate and adsorbent active sites.

The fitting of these models to experimental data will be assessed based on the coefficient of determination (R^2) to ensure statistical reliability. Additionally, the calculated equilibrium adsorption capacities (q_e,cal) from each model will be compared with the experimentally determined values (q_e,exp) to confirm the suitability of the model. The model showing higher R^2, and the closest agreement between q_e,exp and q_e,cal will be considered the best fit, providing insight into the dominant adsorption mechanism.

$$\ln(q_e - q_t) = \ln(K_1 q_e) - K_1\, t \tag{4}$$

$$\frac{t}{q_t} = \frac{1}{K q_e{}^2} + \frac{t}{q_e} \tag{5}$$

where, qe (mg/g) = equilibrium adsorption capacity,
qt (mg/g) = AC at specified time (t).
K_l = constants for pseudo-second-order kinetic models.

2.6. Adsorption isotherm

Understanding the adsorption mechanism is essential for optimizing the performance of AB in dye removal applications. Isotherm modeling provides critical insights into the interaction between the adsorbate (MB) and the adsorbent (NaOH-AB and $ZnCl_2$-AB), enabling the prediction of AC and surface characteristics. The Langmuir model assumes monolayer adsorption on a homogeneous surface, while the Freundlich model accounts for heterogeneous, multilayer adsorption. Comparing these models helps to identify the dominant adsorption mechanism governing the process.

The best fitting model will be evaluated based on the correlation coefficient (R^2), which indicates the degree of agreement between experimental and model predicted values. The model that exhibits the highest R^2 value will be considered the most appropriate representation of the adsorption behaviour.

$$\frac{C_e}{q_e} = \frac{1}{q_m K_L} + \frac{C_e}{q_m} \tag{6}$$

$$\ln(q_e) = \ln(K_F) + \frac{1}{n}\ln(C_e) \tag{7}$$

where, qm = maximum adsorption capacity (mg/g)
K_L= Langmuir affinity constant (l/mg)
K_F = Freundlich constant
n = heterogeneity factor in the Freundlich model.

2.7. Regeneration and reuse of AB

This study aims to enhance the sustainability and cost effectiveness of wastewater treatment by developing regenerable AB from agricultural waste. Evaluating regeneration and reuse performance ensures long term applicability and economic viability of the adsorbent for large scale water purification. Thus, regeneration and reuse studies were performed to evaluate the recyclability of NaOH-AB and $ZnCl_2$-AB. After MB adsorption under optimized conditions, the AB was separated from the treated solution by filtration. The spent AB was then soaked in 50 mL of 0.1 N methanol and thoroughly washed with distilled water to remove residual dye. The cleaned adsorbent was oven dried for 12 h and reused for up to five consecutive adsorption cycles.

3. Result and discussion

3.1. Characterization of raw biomass

Proximate analysis of PPSW was conducted, and the results are presented in Table 3. The raw biomass exhibited a fixed carbon content of 14.85 %, confirming its potential for conversion into biochar through pyrolysis. A higher fixed carbon content is desirable as it contributes to greater char yield and enhanced structural integrity after devolatilization. The removal of moisture and volatile matter further concentrates the carbon matrix, which is essential for subsequent activation processes. The carbon rich framework provides a stable base for developing porous structures and active sites during chemical activation, which are critical for improving adsorption performance. These results align well with previously reported findings on the proximate composition of PPSW [10], reinforcing its suitability as a feedstock for AB synthesis aimed at wastewater treatment applications.

3.2. Characterization of AB

3.2.1. FESEM and EDX analysis

The synthesized NaOH-AB and $ZnCl_2$-AB were oven dried for 24 h prior to FESEM-EDX analysis. The FESEM micrographs (Fig. 1) highlight significant morphological differences between raw PPSW and chemically ABs. The raw PPSW (Fig. 1a) shows a relatively smooth surface with limited porosity, primarily due to partial removal of volatile matter during carbonization. In contrast, NaOH-AB (Fig. 1b) exhibits numerous well developed micropores, which substantially increase the surface area and adsorption potential. This enhanced porosity can be attributed to NaOH strong alkaline nature, which promotes chemical etching and structural disintegration, creating more active sites for adsorption. Similarly, $ZnCl_2$-AB (Fig. 1c) demonstrates an interconnected porous network, indicating effective penetration of $ZnCl_2$ within the biochar matrix. $ZnCl_2$, acting as a Lewis acid, facilitates dehydration and controlled carbonization, preserving the structural integrity while generating high porosity. These morphological improvements explain the superior MB removal achieved by both NaOH-AB and $ZnCl_2$-AB.

The activation process was further confirmed by EDX analysis (Fig. 2). Raw PPSW exhibited a composition dominated by carbon (91.64 %) and oxygen (8.09 %), with traces of potassium (0.27 %). After activation, notable compositional changes were observed: NaOH-AB showed 80.34 % carbon, 18.66 % oxygen, and 1.0 % sodium, whereas $ZnCl_2$-AB contained 87.81 % carbon, 11.37 % oxygen, along with chloride (1.9 %) and zinc (0.60 %). These changes confirm the incorporation of activating agents and the development of new functional groups that enhance surface reactivity. The presence of sodium and zinc indicates successful impregnation, which, coupled with increased porosity, improves AC.

Overall, FESEM-EDX analysis validates that chemical activation with NaOH and $ZnCl_2$ significantly modifies the surface morphology and elemental composition of PPSW derived biochar, leading to improved textural characteristics and functional properties essential for efficient dye adsorption.

Table 3
Proximate analysis of PPSW.

Material	Moisture Content (%)	Volatile Content (%)	Ash (%)	Fixed Carbon (%)
Pigeon pea stalk	8.02	70.50	6.63	14.85

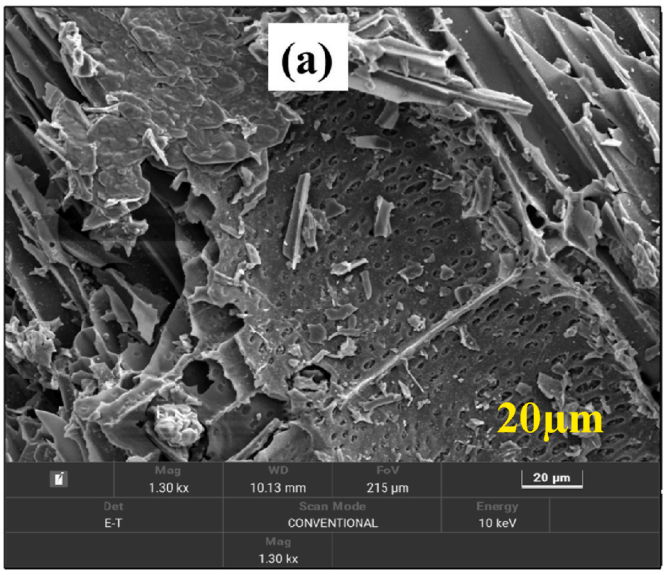

Fig. 1a. FESEM of PPSW-AB.

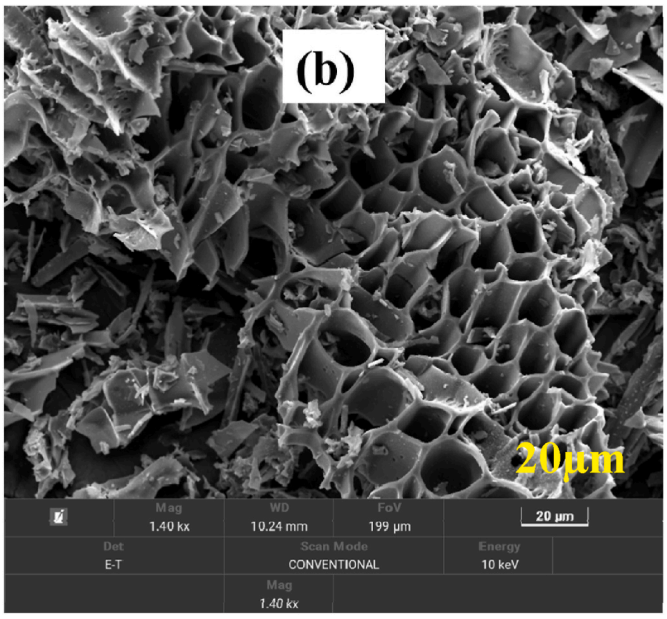

Fig. 1b. FESEM of NaOH -AB

3.2.2. XRD analysis

The structural characteristics and crystalline nature of raw PPSW and chemically ABs (NaOH-AB and $ZnCl_2$-AB) were analyzed using XRD. The raw PPSW exhibited broad peaks at 2θ values of 23.22°, 26.89°, and 29.07°, indicating its predominantly amorphous carbonaceous structure. In contrast, NaOH-AB displayed distinct peaks at 24.56°, 27.57°, 29.25°, 31.03°, and 32.55°, reflecting structural modifications due to sodium incorporation. Similarly, $ZnCl_2$-AB showed well-defined peaks at 11.11°, 20.25°, 23.06°, 25.53°, 26.06°, 27.84°, 29.23°, and 31.30°, suggesting enhanced crystallinity and mineral formation. The presence of these sharp and intense peaks, particularly in $ZnCl_2$-AB, confirms that $ZnCl_2$ acts as an effective activating agent by promoting pore formation and structural reorganization (Fig. 3). Overall, the chemical activation significantly improved crystallinity and structural order compared to the amorphous nature of raw PPSW, owing to rearrangement of carbon structures during activation.

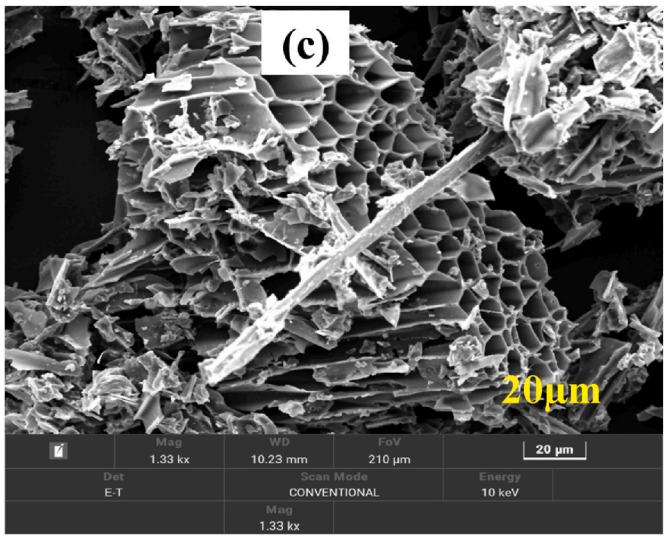

Fig. 1c. FESEM of $ZnCl_2$ - AB

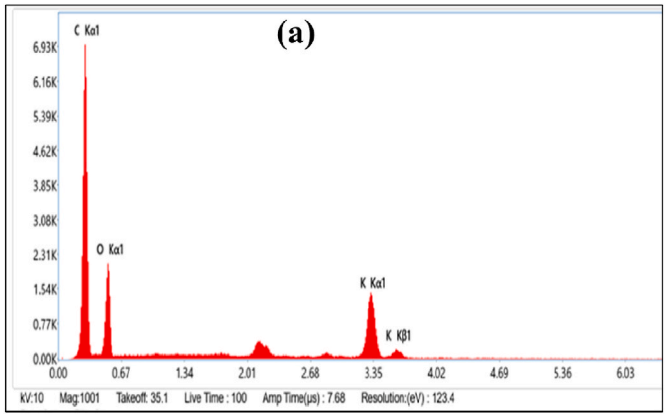

Fig. 2a. EDX of PPSW-AB.

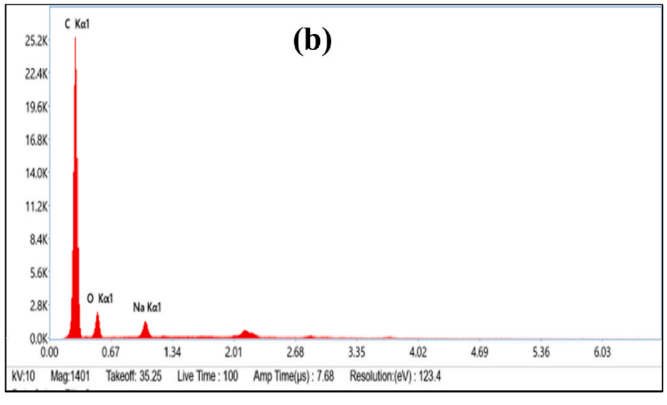

Fig. 2b. EDX of NaOH-AB.

3.2.3. FTIR analysis

FTIR analysis was performed to identify the presence and variations in functional groups of NaOH-AB and $ZnCl_2$-AB, as shown in Fig. 4. The observed peaks provide insights into the chemical functionalities of the AB. Broad peaks around 3650–3680 cm^{-1} indicate O–H stretching vibrations of hydroxyl groups. Peaks near 3061–3068 cm^{-1} correspond to C–H stretching, while those around 1587–1599 cm^{-1} suggest C=C

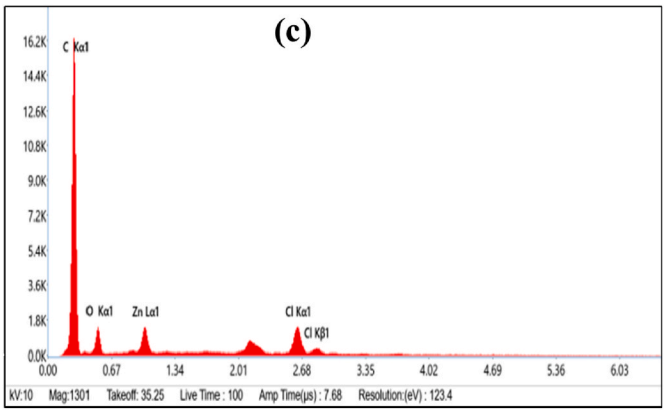

Fig. 2c. EDX of $ZnCl_2$-AB.

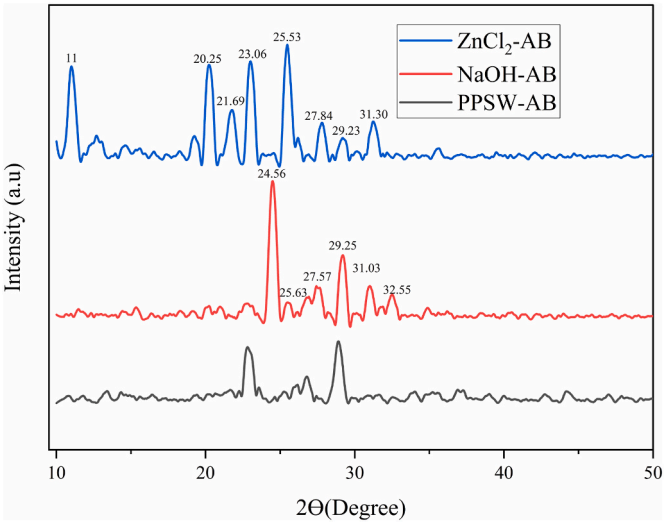

Fig. 3. XRD patterns of AB.

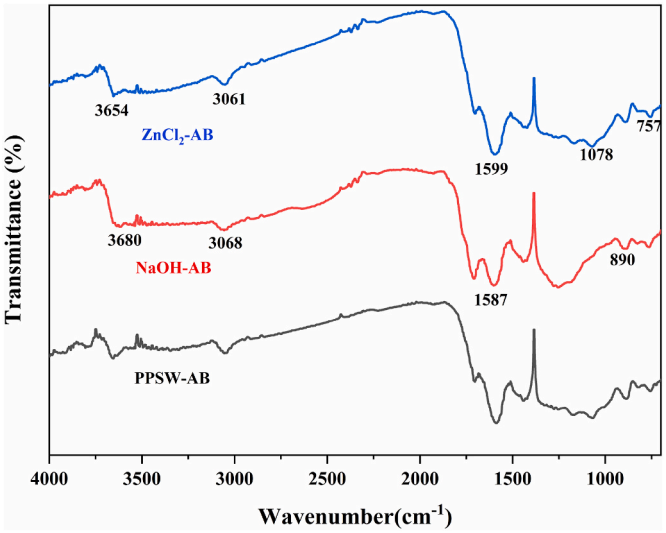

Fig. 4. FTIR patterns of AB.

stretching, indicating the possible formation of carboxyl groups or conjugated structures after activation. Additionally, peaks near 1078 cm^{-1} and 890 cm^{-1} are associated with C–O–C and C–O stretching vibrations, respectively, signifying the presence of aromatic or aliphatic structures. Thus, the FTIR analysis confirmed that the functional groups changes on the surface reflects successful synthesis of AB.

3.2.4. BET analysis

BET surface area analysis revealed a remarkable improvement in the textural properties of AB after chemical activation, underscoring its enhanced suitability as an adsorbent. The surface area of raw PPSW was relatively low (25.42 m^2/g), but increased more than two-fold with NaOH activation (53.83 m^2/g) and over four-fold with $ZnCl_2$ activation (110.23 m^2/g). This enhancement was accompanied by a significant rise in pore volume, from 0.453 cc/g in raw PPSW to 4.22 cc/g (NaOH-AB) and 3.85 cc/g ($ZnCl_2$-AB). Such improvements directly reflect the effectiveness of the activation treatments. NaOH induces chemical etching that generates new pore structures, while $ZnCl_2$ acts as a dehydrating agent, facilitating the development of a more open and porous framework.

Importantly, the pore diameters of 2.33 nm (NaOH-AB) and 2.78 nm ($ZnCl_2$-AB) fall within the mesoporous range (2–50 nm), which is particularly advantageous for the adsorption of MB molecules. This mesoporosity not only improves accessibility of active sites but also supports higher diffusion rates during adsorption. The BET isotherms (Fig. S1 and S2) further confirm the coexistence of micropores and mesopores, as indicated by the combination of Type-I and Type-IV profiles. Collectively, these findings demonstrate that chemical activation substantially enhances surface area, pore volume, and pore structure, translating into superior AC and efficiency for dye removal applications.

3.2.5. Raman Spectroscopy

Raman spectroscopy of the raw biomass and prepared biochar (Fig. 5) shows the typical carbonaceous fingerprint with prominent peaks at ~1350 cm^{-1} (D-band) and ~1580 cm^{-1} (G-band). The presence of a well defined D-band indicates a high density of structural defects and disordered sp^2 carbon domains, while the G-band reflects the development of more ordered graphitic structures. Importantly, the change in relative intensity ratio in the biochar, demonstrating that activation treatment enhanced defect sites while simultaneously promoting partial graphitization. This structural evolution is beneficial because defect rich domains provide more active binding sites, while graphitic regions contribute to electronic conductivity and structural stability. Together, these features explain the improved adsorption potential of the prepared biochar and highlight its suitability for environmental and energy related applications.

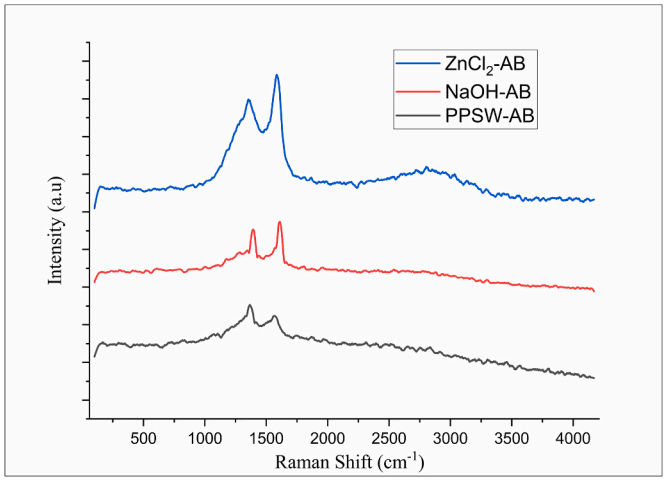

Fig. 5. Raman spectroscopy AB

3.3. ANOVA and statistical analysis

To identify the most influential parameters governing biochar performance, an L9 orthogonal array design was employed and the results were analyzed using ANOVA. This statistical approach enabled the quantification of how activation temperature, activation time, and reagent to carbon ratio affected AC and RE of MB. The ANOVA results clearly demonstrated the robustness of the model. For NaOH-AB, a high F-value of 127.47 for AC (sum of squares = 0.124) and 173.51 for RE highlighted the strong statistical significance of the process parameters (Tables 4a and 4b). The corresponding low probabilities of error (0.78 % for AC and 0.57 % for RE) confirm that the observed trends were not due to noise. Importantly, all P values were well below the threshold of 0.005, further validating the model predictive strength. Among the tested factors, activation temperature, activation time, and reagent to carbon ratio consistently emerged as significant parameters influencing adsorption performance. This finding underscores that both thermal activation and chemical environment critically govern surface chemistry and pore structure development, which in turn determine MB adsorption.

Overall, the integration of orthogonal array design with ANOVA provides a statistically validated framework for optimizing AB synthesis. The strong correlation between experimental and predicted outcomes confirms that the adopted methodology not only explains current results but also offers a reliable pathway for scaling and fine-tuning biochar synthesis toward maximum dye RE.

The ANOVA results (Table 5) confirm that the developed model for $ZnCl_2$-AB synthesis is statistically significant and reliable for predicting MB removal performance. The high F test value (26.43) and corresponding sum of squares (0.0123) indicate a strong explanatory power of the model. Importantly, the probability of obtaining such F values due to random noise is very low: only 3.69 % for AC and 0.97 % for RE. These low p values highlight that the observed effects are not incidental but are strongly associated with the chosen process variables. Furthermore, the adequate signal to noise ratio validates the robustness of the model, ensuring its effectiveness in guiding the optimization of AC and RE. Overall, these results demonstrate that $ZnCl_2$-AB can be reliably optimized through the proposed statistical model to achieve enhanced dye removal performance.

The statistical validation of the NaOH-AB synthesis model is presented in Table 6. The predicted R^2 values (0.9974 for AC and 0.9981 for RE) were in strong agreement with the adjusted R^2 values (0.9896 and 0.9923, respectively), with differences of less than 0.2. This close alignment confirms the robustness and reliability of the developed models. The correlation coefficient (C.R.) values, approaching unity, further indicate the model strong predictive capability and its ability to capture the variability in the experimental responses. The reliability of the models was also supported by their precision metrics. The low coefficients of variance (0.1722 for AC and 0.1143 for RE) and standard deviations (0.0128 for AC and 0.1129 for RE) indicate minimal experimental error and high reproducibility. Moreover, the Adequate Precision values (36.373 for AC and 38.167 for RE) far exceeded the acceptable threshold of 4, signifying an excellent signal to noise ratio and confirming the models suitability for reliable prediction of the responses [37].

Overall, these statistical indicators collectively demonstrate that the Taguchi models for NaOH-AB synthesis are statistically sound, predictive, and capable of guiding process optimization with high accuracy.

A statistical evaluation of the batch experiments for $ZnCl_2$-AB is presented in Table 7, highlighting the predictive strength and robustness of the developed models. The predicted R^2 values for AC and RE were 0.7478 and 0.9346, respectively, showing strong alignment with the adjusted R^2 values of 0.9502 (AC) and 0.9871 (RE). The narrow difference (<0.2) between predicted and adjusted R^2 underscores the high predictive reliability of the models. In addition, the coefficient of regression (C.R.) values approached unity, confirming that the models accurately captured both the mean response trends and underlying variability. The low coefficients of variation (C.V.) and standard deviations 0.1184 and 0.0088 for AC, and 0.0647 and 0.0643 for RE further highlight the precision and consistency of the predictions. The Adequate Precision ratios of 14.142 (AC) and 26.102 (RE), far exceeding the threshold of 4, indicate that the models possess a strong signal to noise ratio, enabling effective navigation of the design space. These values collectively demonstrate that the chosen Taguchi L9 orthogonal array design provides not only statistically valid models but also reliable optimization pathways for tailoring activation parameters. Overall, the results establish that the NaOH-AB and $ZnCl_2$-AB can be optimized with high confidence, ensuring enhanced adsorption performance and offering a robust basis for process scale-up and practical applications.

Table 4
ANOVA for chosen model and process parameters for NaOH-AB.

a. Adsorption Capacity						
Source	Sum of squares	df	Mean square	F-value	P-value	
Model	0.1249	6	0.0208	127.47	0.0078	significant
A Activation temperature	0.0098	2	0.0049	30.00	0.0323	
B Activation time	0.0364	2	0.0182	111.33	0.0089	
C Reagent to carbon ratio	0.0788	2	0.0394	241.09	0.0041	
Residual	0.0003	2	0.0002			
Cor total	0.1253	8				
b. Removal Efficiency						
Model	13.27	6	2.21	173.51	0.0057	significant
A Activation temperature	0.4939	2	0.2469	19.38	0.0491	
B Activation time	4.11	2	2.06	161.33	0.0062	
C Reagent to carbon ratio	8.66	2	4.33	339.81	0.0029	
Residual	0.0255	2	0.0127			
Cor total	13.29	8				

Table 5
ANOVA for chosen model and process parameters for $ZnCl_2$ -AB.

a. Adsorption Capacity						
Source	Sum of squares	Df	Mean square	F-value	P-value	
Model	0.0123	6	0.0021	26.43	0.0369	significant
A Activation temperature	0.0023	2	0.0011	14.71	0.0636	
B Activation time	0.0078	2	0.0039	49.86	0.0197	
C Reagent to carbon ratio	0.0023	2	0.0011	14.71	0.0636	
Residual	0.0002	2	0.0002			
Cor total	0.0125	8				
b. Removal Efficiency						
Model	2.55	6	0.4250	102.83	0.0097	significant
A Activation temperature	0.5419	2	0.2709	65.55	0.0150	
B Activation time	1.54	2	0.7689	186.03	0.0053	
C Reagent to carbon ratio	0.4704	2	0.2352	56.90	0.0173	
Residual	0.0083	2	0.0041			
Cor total	2.56	8				

Table 6
Statistical parameter analysis obtained from ANOVA study for NaOH-AB.

a. Adsorption Capacity				b. Removal Efficiency		
Standard Deviation	0.0128	R^2	0.9974	0.1129	R^2	0.9981
Mean	7.42	Adjusted R^2	0.9896	98.81	Adjusted R^2	0.9923
Coefficient of variance	0.1722	Predicted R^2	0.9472	0.1143	Predicted R^2	0.9612
		Adeq Precision	36.3732		Adeq Precision	38.1676

Table 7
Statistical parameter analysis obtained from ANOVA study for $ZnCl_2$-AB.

a. Adsorption Capacity				b. Removal Efficiency		
Standard Deviation	0.0088	R^2	0.9875	0.0643	R^2	0.9968
Mean	7.45	Adjusted R^2	0.9502	99.39	Adjusted R^2	0.9871
Coefficient of variance	0.1184	Predicted R^2	0.7478	0.0647	Predicted R^2	0.9346
		Adeq Precision	14.1429		Adeq Precision	26.1026

3.4. Parametric effects on Adsorption Capacity (AC) and removal efficiency (RE)

Activation parameters including temperature, time, and reagent to carbon (R/C) ratio play decisive roles in tuning the porosity and surface chemistry of activated AB, thereby governing its AC and REtowards MB. Using an L9 orthogonal array design, we systematically evaluated these parameters and identified distinct activation behaviours for NaOH-AB and $ZnCl_2$-treated AB.

3.4.1. Effect of activation temperature

Temperature exerted opposite influences on the two activation systems. NaOH-AB exhibited its highest AC (7.54 mg/g) and complete dye removal at the lowest temperature (40°C), beyond which both AC and RE declined as shown in Fig. 6A and 7A. This suggests that low temperature activation effectively preserves oxygenated functional groups and micropores essential for MB adsorption, while higher temperatures promote structural collapse and pore shrinkage.

In contrast, $ZnCl_2$-AB benefited from elevated temperatures, with AC steadily increasing up to 7.51 mg/g at 80°C, where complete removal of

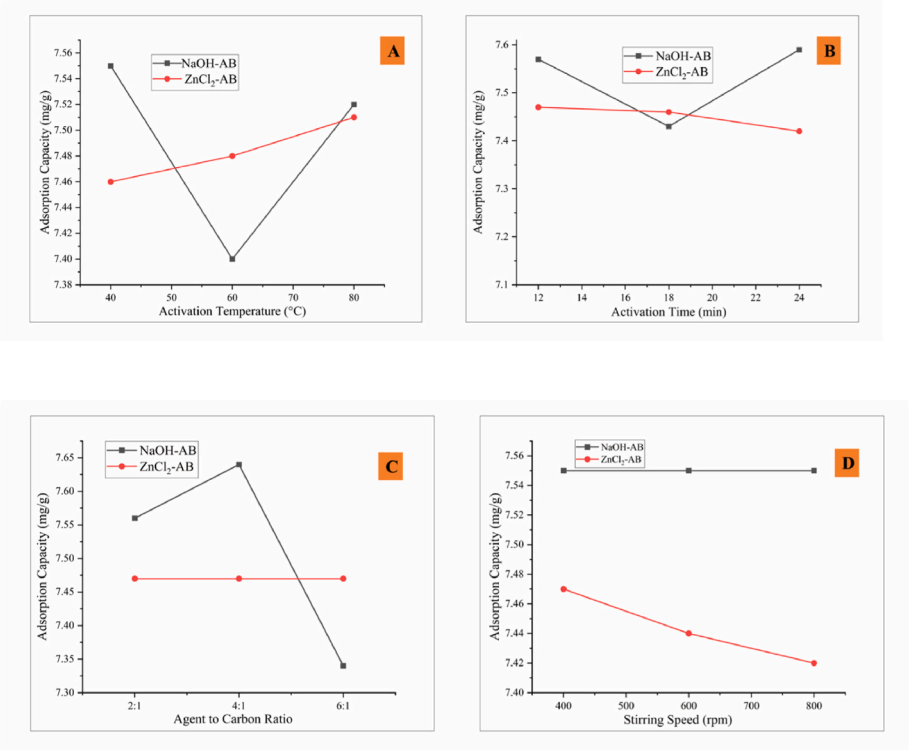

Fig. 6. A. Effect of parameters on AC. A. Activation temperature B. Activation time C. Agent to carbon ratio D. Stirring speed. (NaOH-AB & $ZnCl_2$-AB).

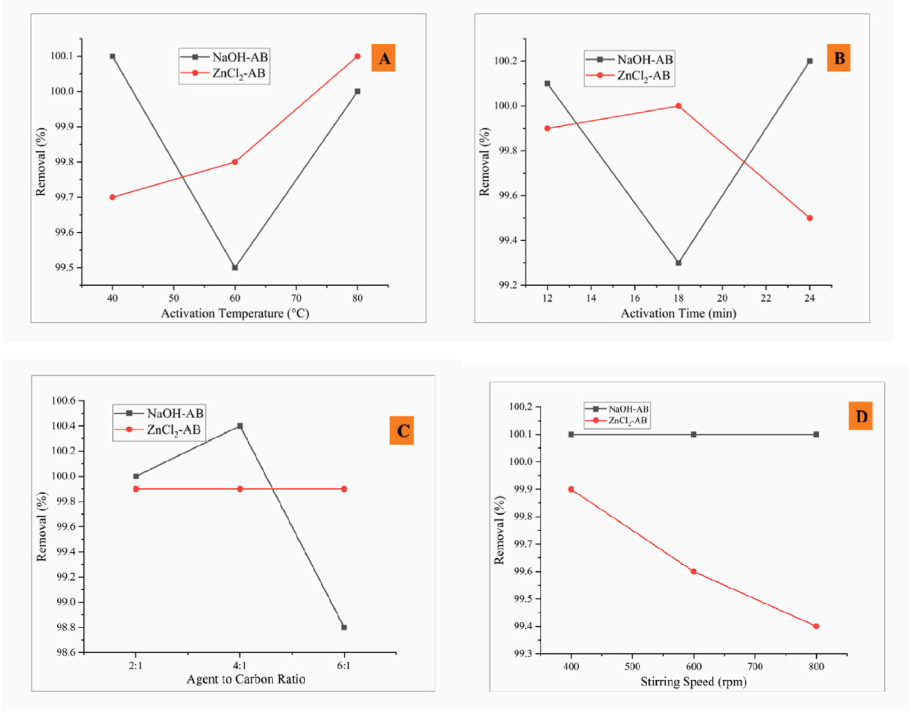

Fig. 7. A. Effect of parameters on RE. A. Activation temperature B. Activation time C. Agent to carbon Ratio D. Stirring speed. (NaOH-AB & $ZnCl_2$-AB).

MB was achieved. This enhancement reflects the Lewis acid mechanism of $ZnCl_2$, where higher temperatures accelerate dehydration and aromatization, facilitating micropore generation and stable carbon frameworks. Taken together, these contrasting trends highlight that alkali activation (NaOH) favours mild thermal conditions to retain surface functionality, whereas $ZnCl_2$ activation requires higher temperatures to fully exploit its pore forming potential.

3.4.2. *Effect of activation time*

Activation duration was found to be the most influential factor. NaOH-AB reached optimal performance (AC = 7.54 mg/g, RE = 100 %) at 12 h, but prolonged treatment (18 h) led to overetching and collapse of micropores, reducing adsorption sites. Interestingly, a recovery in both AC and RE at 24 h suggests secondary pore stabilization or functional group rearrangement. For $ZnCl_2$-AB, maximum AC (7.48 mg/g) was observed at 18 h, beyond which both AC and RE declined due to pore coalescence and possible tar deposition as evident from Fig. 6B and 7B. The temporal evolution underscores that over activation does not linearly enhance adsorption; rather, an optimal window must balance pore development with structural integrity.

3.4.3. *Effect of reagent-to-carbon ratio*

The R/C ratio critically influenced NaOH activation but had negligible effect on $ZnCl_2$ activation. For NaOH-AB, an intermediate ratio of 4:1 yielded the highest AC (7.5 mg/g) and 100 % RE, while excessive reagent loading (6:1) caused pore blockage and loss of surface area. The effect of R/C ratio on AC and RE is depicted in Fig. 6C and 7C. Conversely, $ZnCl_2$-AB maintained nearly constant AC (~7.45 mg/g) and stable RE across all tested ratios, reflecting the milder and more controlled nature of Lewis acid activation.

3.4.4. *Effect of stirring speed*

Stirring speed had little effect on NaOH-AB, with AC remaining nearly constant between 400 and 800 rpm as indicated in Fig. 6D and 7D. $ZnCl_2$-AB, however, showed a slight decline in AC and RE at higher speeds, possibly due to turbulence-induced desorption and reduced adsorbate–adsorbent contact time.

The 3-D response surafce plots for AC and RE are shown in Fig. S3 (a-d). Collectively, these results demonstrate that NaOH activation is highly sensitive to both temperature and reagent loading, requiring milder conditions (40°C, 12 h, 4:1 ratio) to maximize adsorption, while $ZnCl_2$ activation benefits from higher temperatures (80°C) and longer durations (18 h) to fully develop microporous structures. The identification of these distinct activation pathways is critical for tailoring biochar properties for targeted water treatment applications.

3.5. *Prediction of optimum condition*

The synthesis of NaOH-AB and $ZnCl_2$-AB from PPSW was strongly influenced by activation temperature, time, ragent to carbon ratio, and stirring speed parameters that govern pore structure and surface chemistry, and thus adsorption performance. The optimization strategy aimed to minimize resource inputs while maximizing AC and RE.

NaOH activation performed best at 80 °C, 24 h, a 4:1 agent-to-carbon ratio, and 400 rpm, yielding predicted maxima of 7.56 mg/g AC and 100 % RE (Table 8). In contrast, $ZnCl_2$ achieved nearly equivalent outcomes (7.51 mg/g AC, 99.9 % RE) under less demanding conditions—80 °C, 12 h, 2:1 ratio, and 400 rpm.

These results highlight that while both activators produce highly efficient biochars, $ZnCl_2$ offers significant advantages in terms of shorter activation time and lower reagent consumption. Importantly, this positions $ZnCl_2$-AB as a more sustainable adsorbent option, reinforcing the study's broader goal of developing resource-efficient materials for environmental remediation.

3.6. *Experimental validation of model*

The regression based model was validated by conducting nine confirmatory trials for each AB under optimal synthesis conditions, and the actual experimental results were compared with the predicted values (Table 9). A strong correlation was observed between the predicted and experimental values for MB adsorption and RE, with coefficients of

Table 8
Prediction of optimum condition.

Sr. No.	Reagents	Activation temperature (°C)	Activation time (hrs)	Reagent to carbon ratio	Stirring speed (RPM)	Optimum adsorption (mg/g)	Optimum Removal (%)
1.	NaOH-AB	80	24	4:1	400	7.56	100
2.	$ZnCl_2$-AB	80	24	4:1	400	7.51	99.90

Table 9
Validation of model by experiments.

Sr. No.	Activation temperature	Activation time	Reagent to carbon	Stirring speed	Response I AC		Response II RE	
					Predicted	Actual	Predicted	Actual
1.	80	24	2:1	400	7.56	7.15 (NaOH-AB)	100	96.20 (NaOH-AB)
2.	80	24	2:1	400	7.49	7.38 ($ZnCl_2$-AB)	99.9	98.42 ($ZnCl_2$-AB)

determination (R^2) of 0.98 and 0.99, respectively. These high R^2 values indicate excellent model accuracy and reliability in predicting process outcomes. The confirmatory experiments demonstrated close agreement with the model predictions, confirming that the developed model can effectively guide the optimization of PPSW derived AB. This predictive capability is essential for reducing experimental runs and resource consumption while ensuring process efficiency. The comparison of predicted and experimental values for NaOH-AB and $ZnCl_2$-AB is illustrated in Figs. S4 (a–b) and S5 (a–b), respectively.

3.7. Adsorption kinetics

The adsorption kinetics of MB dye on NaOH-AB and $ZnCl_2$-AB were evaluated using both pseudo-first-order and pseudo-second-order models at different temperatures (30, 40, and 50 °C), as illustrated in Figs. 8a, 8b and Fig. 9a, 9b. The kinetic parameters (q_e, K_1, and K_2) derived from the linearized plots are summarized in Table 10.

A clear distinction emerged between the two models: while the pseudo-first-order model showed lower correlation with the experimental data, the pseudo-second-order model consistently provided excellent agreement. Specifically, the correlation coefficients (R^2) for MB dye adsorption reached 0.99 for both NaOH-AB and $ZnCl_2$-AB across all tested temperatures. Furthermore, the calculated equilibrium adsorption capacities (q_e) from the pseudo-second-order model closely matched the experimental values, reinforcing the reliability of this model in describing the system.

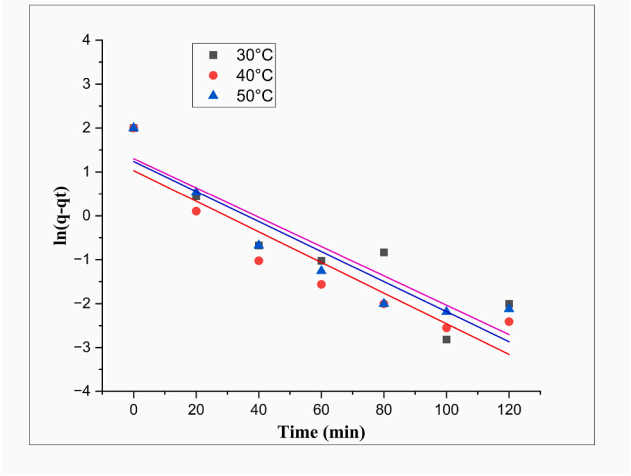

a) Evaluation of MB adsorption on NaOH-AB (Pseudo-first-order Model)

Fig. 8a. Evaluation of MB adsorption on NaOH-AB (Pseudo-first-order Model).

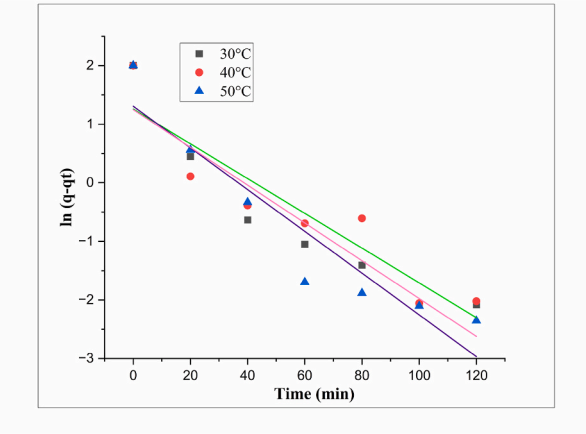

b) Evaluation of MB adsorption on $ZnCl_2$-AB (Pseudo-first-order Model)

Fig. 8b. Evaluation of MB adsorption on $ZnCl_2$-AB (Pseudo-first-order Model).

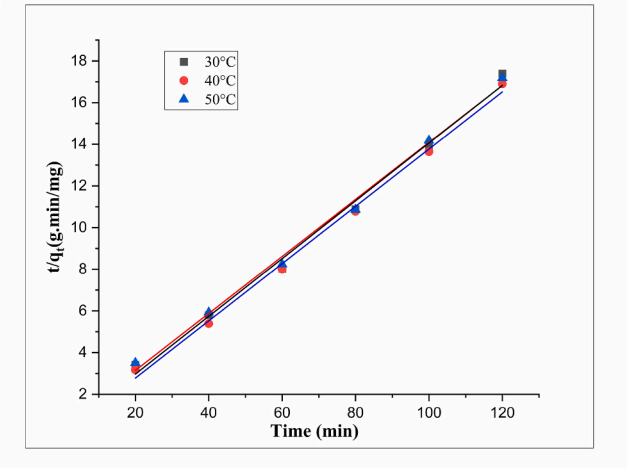

a) Evaluation of MB adsorption on NaOH-AB (Pseudo-second-order Model)

Fig. 9a. Evaluation of MB adsorption on NaOH-AB (Pseudo-second-order Model).

These results highlight that the adsorption mechanism is better represented by the pseudo-second-order kinetics, implying that chemisorption governed by valence forces through electron sharing or

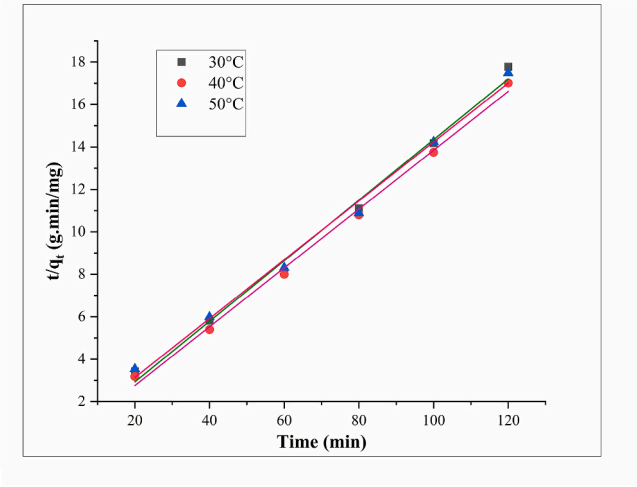

b) Evaluation of MB adsorption on $ZnCl_2$-AB (Pseudo-second-order Model)

Fig. 9b. Evaluation of MB adsorption on $ZnCl_2$-AB (Pseudo-second-order Model).

Table 10
Adsorption kinetics parameters for MB adsorption by NaOH-AB and $ZnCl_2$-AB.

Pseudo-first-order Model (NaOH-AB)				Pseudo-second-order Model (NaOH-AB)		
Temperature (°C)	q (mg/g)	K_1 (h^{-1})	R^2	q (mg/g)	K_2 ($g•h^{-1}•mg^{-1}$)	R^2
30	4.032	0.0334	0.83	7.215	0.096	0.99
40	2.639	0.0349	0.85	7.278	0.616	0.99
50	2.897	0.0342	0.87	7.309	0.045	0.99
$ZnCl_2$-AB				$ZnCl_2$-AB		
30	3.491041	0.0323	0.86	7.115	0.457	0.99
40	3.521194	0.0297	0.89	7.228	2.99	0.99
50	3.697659	0.0356	0.88	6.988	0.103	0.99

exchange plays a dominant role. This mechanistic insight underscores the strong interaction between MB dye molecules and the surface-active sites of the modified biochars, providing a fundamental basis for their high adsorption efficiency.

3.8. Adsorption isotherm

The adsorption behavior of MB on NaOH-AB and $ZnCl_2$-AB was evaluated using Langmuir and Freundlich isotherm models. Both models represented in Fig. 10 and 11 exhibited excellent correlation with the equilibrium data (R^2 values > 0.95), confirming their suitability for describing the adsorption process. This strong statistical fit highlights the reliability of the prepared adsorbents in capturing MB under varying concentrations.

The Langmuir analysis revealed maximum monolayer adsorption capacities (q_m) of 88.49 mg/g for NaOH-AB and 92.5 mg/g for $ZnCl_2$-AB, demonstrating the high efficiency of both activated biochars. The slightly higher capacity of $ZnCl_2$-AB suggests a greater density of uniformly distributed active sites, which enhances surface coverage and contributes to improved dye uptake. These values compare favorably with other reported biochar-based adsorbents, underscoring the competitive performance of the synthesized materials.

Complementing this, the Freundlich model yielded 1/n values < 1, signifying favourable adsorption conditions and the presence of heterogeneous surface interactions. This indicates that both biochars not only provide abundant adsorption sites but also maintain surface heterogeneity, which is advantageous for real world applications where wastewater contains diverse pollutants.

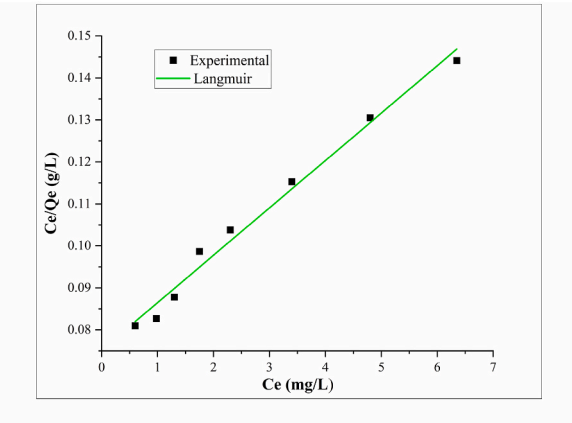

a) Equilibrium Isotherm models for MB adsorption on $ZnCl_2$-AB (Langmuir Model)

Fig. 10a. Equilibrium Isotherm models for MB adsorption on $ZnCl_2$-AB (Langmuir Model).

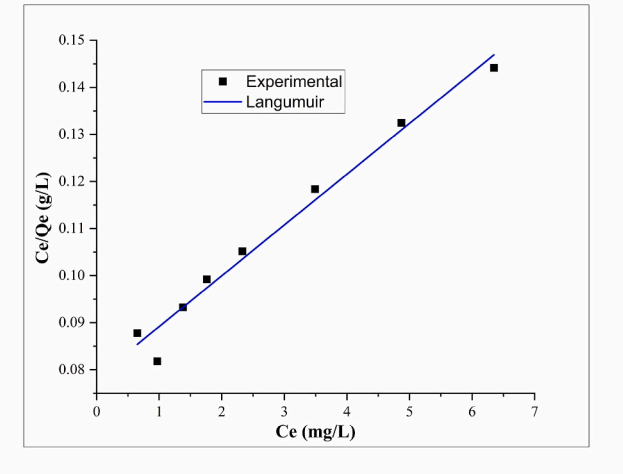

b) Equilibrium Isotherm models for MB adsorption on $ZnCl_2$-AB (Langmuir Model)

Fig. 10b. Equilibrium Isotherm models for MB adsorption on $ZnCl_2$-AB (Langmuir Model).

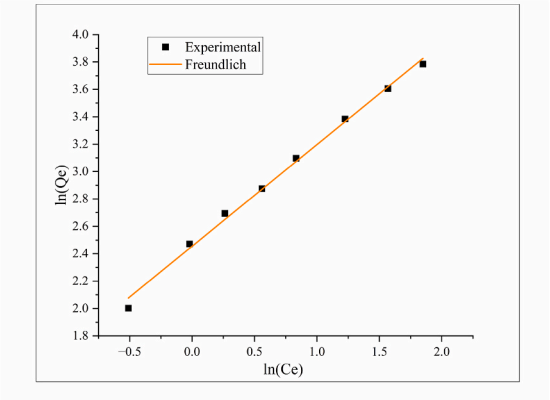

a) Equilibrium Isotherm models for MB adsorption on NaOH-AB (Freundlich Model)

Fig. 11a. Equilibrium Isotherm models for MB adsorption on NaOH-AB (Freundlich Model).

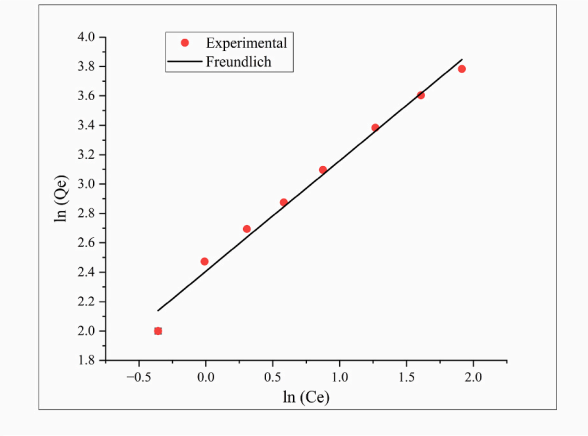

b) Equilibrium Isotherm models for MB adsorption on $ZnCl_2$-AB (Freundlich Model)

Fig. 11b. Equilibrium Isotherm models for MB adsorption on $ZnCl_2$-AB (Freundlich Model).

Table 11
Adsorption Isotherm parameters for MB adsorption by NaOH-AB and $ZnCl_2$-AB.

Langmuir (NaOH-AB)			Freundlich (NaOH-AB)		
q_m (mg/g)	Kl (L/mg)	R^2	K_F (mg/g)	N	R^2
88.49	0.150	0.98	11.64	1.348	0.99
$ZnCl_2$-AB			$ZnCl_2$-AB		
92.59	0.137	0.977	11.10	1.329	0.98

Overall, the integration of both isotherm models illustrates that NaOH-AB and $ZnCl_2$-AB are highly effective adsorbents for dye removal. The combination of strong statistical fit, high monolayer adsorption capacities, and favourable Freundlich parameters underscores their potential for scalable wastewater treatment applications. Figs. 10 and 11 illustrate the linearized Langmuir and Freundlich plots, while the corresponding parameters are summarized in Table 11.

3.9. Mechanism of adsorptive removal of MB

The adsorption of MB, a cationic dye, onto PPSW-AB is governed by multiple synergistic interactions arising from the surface chemistry of the modified adsorbents. The activation treatments (NaOH and $ZnCl_2$) enriched the biochar surface with functional groups such as hydroxyl (–OH), carboxyl (–COOH), carbonyl (C=O), and negatively charged moieties ($–O^-$, COO^-). These functionalities significantly enhanced the affinity of the adsorbent toward MB, as confirmed by the higher RE observed compared to unmodified biochar. Electrostatic attraction was identified as the dominant mechanism, whereby the negatively charged surface groups strongly interacted with the positively charged MB molecules under neutral pH conditions. This charge-driven interaction accounts for the rapid initial adsorption and high uptake capacity of both NaOH-AB and $ZnCl_2$-AB. In addition, hydrogen bonding between the –OH groups of the adsorbents and the nitrogen atoms of MB contributed to stable molecular anchoring. The combined effect of electrostatic attraction and hydrogen bonding was further supported by FTIR and FESEM–EDX analyses, which revealed the presence of MB characteristic peaks on the spent adsorbents and changes in surface morphology after adsorption. The incorporation of sulfonate, hydroxyl, and carboxyl groups thus not only improved surface reactivity but also expanded the range of binding pathways available for MB capture.

Overall, the enhanced adsorption performance of NaOH-AB and $ZnCl_2$-AB demonstrates that targeted surface modification of agricultural residue-derived biochar can effectively tailor functional groups to maximize dye removal efficiency. This highlights the potential of PPSW derived adsorbents as sustainable and efficient materials for wastewater treatment.

3.10. Regeneration and reusability studies of AB

To assess the sustainability of AB in water treatment applications, the regeneration performance of NaOH-AB and $ZnCl_2$-AB was evaluated over five consecutive adsorption desorption cycles for MB removal. Both adsorbents demonstrated stable performance with only a slight decline in efficiency after each cycle. After five regeneration cycles, MB removal decreased by approximately 15 % for NaOH-AB and 17 % for $ZnCl_2$-AB compared to the initial values as shown in Fig. S6.

This minimal loss in performance highlights the excellent recyclability and robustness of both AB types, indicating their potential for real time, long-term application. The consistent performance across multiple cycles suggests that structural integrity and functional groups were largely preserved during regeneration. Reusability not only enhances economic feasibility by reducing material replacement costs but also minimizes secondary waste generation, aligning with sustainable water treatment objectives.

4. Comparison with other studies

A comparative assessment of the developed AB from PPSW with previously reported adsorbents is presented in Table 12. Conventional adsorbents derived from papaya peel, areca nut husk, grape pomace, and rubber seed pericarp biomass achieved MB removal efficiencies ranging from 92.4 % to 96.5 % [38–41]. While these values indicate good adsorption capability, the PPSW based AB synthesized in the present study exhibited superior performance, achieving 100 % and 99.9 % RE for NaOH-AB and $ZnCl_2$-AB, respectively.

In addition to RE, the current study addressed critical aspects often overlooked in previous works, such as cost estimation and sustainability evaluation. The production cost of PPSW derived AB was estimated at $4.037 for NaOH-AB and $4.246 for $ZnCl_2$-AB, which is relatively low compared to commercial adsorbents and competitive with other biomass-based materials. Previous studies typically focused on demonstrating adsorption efficiency without providing a detailed economic analysis limiting their applicability for large-scale implementation.

The superior performance and cost-effectiveness of PPSW based AB can be attributed to two major factors: (i) dual chemical activation using strong alkaline (NaOH) and Lewis acidic ($ZnCl_2$) agents, which enhanced surface porosity, generated abundant functional groups, and increased adsorption sites; and (ii) Taguchi-based optimization, which systematically minimized experimental runs while identifying dominant process parameters influencing activation. This approach ensured maximum RE with minimal chemical and energy consumption, thereby reducing overall production costs.

Furthermore, the integration of economic evaluation with adsorption performance differentiates this study from conventional works. While most reported studies focus solely on removal capability, the present work emphasizes scalability and sustainability by combining high RE, cost analysis, and reusability performance. Thus, PPSW derived AB not only offers superior adsorption characteristics but also provides a practical and economically viable solution for wastewater treatment in real-world applications.

5. Cost analysis

In large scale production of AB, the economics of the process are strongly dependent on the cost of raw biomass and the optimization of activation conditions. The use of locally available agricultural residues, such as PPSW, provides a cost advantage by eliminating transportation and procurement expenses associated with conventional feedstocks. Moreover, valorizing agricultural waste into value-added adsorbents promotes circular economy practices and mitigates environmental

Table 12
Comparison of the RE of NaOH-AB and $ZnCl_2$-AB towards MB with other materials.

Sr. No.	Feedstock	Activating agent	Method	RE (%)	Cost	References
1.	Papaya Peel	H_3PO_4	Adsorption	92.4	NA	[38]
2.	Areca Nut Husk	MnO-NiO-ZnO	Adsorption	93.05	NA	[39]
3.	Rubber seed pericarp biomass	H_3PO_4	Adsorption	96.5	NA	[40]
4.	Grape pomace	–	Adsorption	96	NA	[41]
5.	Bovine serum albumin nanosorbent	–	Adsorption (polymer material)	69	NA	[42]
7.	PPSW	NaOH	Adsorption	100	$4.037/Kg	Present study
8.	PPSW	$ZnCl_2$	Adsorption	99.9	$4.246/Kg	Present study

issues like open-field residue burning. However, the overall cost of AB preparation is not limited to feedstock availability; it is also influenced by the type and quantity of activating chemicals, the activation methodology employed (e.g., chemical activation with NaOH or $ZnCl_2$), operating conditions such as temperature and time, and energy requirements for drying, carbonization, and calcination. These variables collectively impact both capital expenditure (CAPEX) and operational expenditure (OPEX). For a realistic estimation of economic feasibility, all material costs in this study were considered at industrial-grade prices. Additionally, the optimized synthesis conditions derived from the Taguchi design of experiments not only enhance adsorption performance but also reduce energy and chemical consumption, thereby improving cost-effectiveness and scalability of the process. Thus, the detailed cost analysis part considering all the contributions are given below:

Cost of Deionized water (2 L) = $0.25.

Cost of raw PPSW (1.666 Kg) = $0.2.

Cost of drying for PPSW = Hours*unit*cost per unit = 12*1*0.077 = $0.924.

Cost of carbonization of PPSW = Hours*unit*cost per unit = 2*2*0.077 = $0.308.

Total cost for AB (833.33 gm) = $1.682.

Cost of NaOH (416.67 gm) = $0.14.

Cost of $ZnCl_2$ (416.67 gm) = $0.33.

Cost of agitation for AB = Hours*unit*cost per unit = 24*1*0.077 = $1.848.

Net cost for NaOH-AB (1 kg) = 1.682 + 0.14 + 1.848 = $3.67.

Overhead cost for NaOH-AB = 10 % of net cost = $0.367.

Total cost for NaOH AB = Overhead cost + Net cost = $4.037.

Net cost for $ZnCl_2$-AB (1 kg) = 1.682 + 0.33 + 1.848 = $3.86.

Overhead cost for $ZnCl_2$-AB = 10 % of net cost = $0.386.

Total cost for $ZnCl_2$-AB = Overhead cost + Net cost = $4.246.

6. Conclusion

This study successfully demonstrated the synthesis and optimization of AB from PPSW using NaOH and $ZnCl_2$ as activating agents, employing the Taguchi L9 orthogonal array approach to systematically evaluate key process variables. Four critical factors activation temperature, activation time, reagent to carbon ratio, and stirring speed were analyzed for their influence on AC and RE of MB dye from aqueous solutions.

The optimized conditions for both NaOH-AB and $ZnCl_2$-AB were found to be an activation temperature of 80 °C, activation time of 12 h, reagent to carbon ratio of 2:1, and stirring speed of 400 rpm. Under these conditions, the NaOH-AB exhibited an AC of 7.56 mg/g and 100 % RE, while the $ZnCl_2$-AB achieved an AC of 7.51 mg/g with complete MB removal. Statistical analysis indicated that activation temperature and reagent to carbon ratio exerted the most significant impact on performance metrics, primarily due to their influence on pore development, surface area enhancement, and functional group distribution. The improved adsorption performance can be attributed to the synergistic effects of chemical activation and carbonization under optimized conditions. NaOH, acting as a strong base, facilitated chemical etching and enhanced microporosity, while $ZnCl_2$, functioning as a Lewis acid, promoted dehydration and structural stabilization, thereby increasing surface area and preserving pore integrity. These mechanisms collectively contributed to high dye uptake efficiency, supported by experimental validation and ANOVA based statistical robustness of the predictive model.

Beyond adsorption performance, this work demonstrates the potential of agricultural residues, specifically PPSW, as a sustainable precursor for high value adsorbents, aligning with circular bioeconomy principles. The cost analysis revealed cost effectiveness of the synthesized AB with $4.037/Kg $4.246/Kg for NaOH-AB and $ZnCl_2$-AB. Moreover, the adsorbents also shown good stability in reuse with 15–17 % decrease in RE after five consecutive cycles. In summary, PPSW derived AB activated with NaOH and $ZnCl_2$ under optimized conditions offers an environmentally benign, cost effective, and technically viable solution for wastewater remediation. Future work could extend this approach to multi-contaminant systems and real industrial effluents, while integrating life cycle and techno economic assessments to further validate large-scale applicability.

CRediT authorship contribution statement

Shubhangi Umare: Writing – original draft, Methodology, Investigation, Formal analysis, Data curation. **Ajay K. Thawait:** Supervision, Resources, Project administration, Conceptualization. **Sumit H. Dhawane:** Writing – review & editing, Supervision, Software, Resources, Project administration, Data curation, Conceptualization.

Consent to participant

Not Applicable.

Ethical approval

Not Applicable.

Consent for publication

All respective authors read and permitted the final manuscript.

Funding

Not Applicable.

Competing of interest

The authors declare no competing interests.

Acknowledgement

The authors gratefully acknowledge the use of the Raman Spectroscopy Facility (IndiRam CTR-300), developed under the NMITLI Project by CSIR-AMPRI, Bhopal.

Appendix A. Supplementary data

Supplementary data to this article can be found online at https://doi.org/10.1016/j.biombioe.2025.108385.

Data availability

No data was used for the research described in the article.

References

[1] A. Saravanan, P.R. Yaashikaa, P. Senthil Kumar, A.S. Vickram, S. Karishma, R. Kamalesh, G. Rangasamy, Techno-economic and environmental sustainability prospects on biochemical conversion of agricultural and algal biomass to biofuels, J. Clean. Prod. 414 (2023) 137749, https://doi.org/10.1016/j.jclepro.2023.137749.

[2] M. Tan, Conversion of agricultural biomass into valuable biochar and their competence on soil fertility enrichment, Environ. Res. 234 (2023) 116596, https://doi.org/10.1016/j.envres.2023.116596.

[3] S. Umare, A.K. Thawait, S.H. Dhawane, Remediation of arsenic and fluoride from groundwater : a critical review on bioadsorption , mechanism , future application , and challenges for water purification, Environ. Sci. Pollut. Res. (2024), https://doi.org/10.1007/s11356-024-33679-y.

[4] S. Bhuvaneshwari, H. Hettiarachchi, J.N. Meegoda, Crop residue burning in India: policy challenges and potential solutions, Int. J. Environ. Res. Publ. Health 16 (2019), https://doi.org/10.3390/ijerph16050832.

[5] S.K. Lohan, H.S. Jat, A.K. Yadav, H.S. Sidhu, M.L. Jat, M. Choudhary, J.K. Peter, P. C. Sharma, Burning issues of paddy residue management in north-west states of India, Renew. Sustain. Energy Rev. 81 (2018) 693–706, https://doi.org/10.1016/j.rser.2017.08.057.

[6] A.K. Sakhiya, P. Kaushal, V.K. Vijay, Process optimization of rice straw-derived AB and biosorption of heavy metals from drinking water in rural areas, Appl. Surf. Sci. Adv. 18 (2023) 100481, https://doi.org/10.1016/j.apsadv.2023.100481.

[7] A.G. Adeniyi, K.O. Iwuozor, E.C. Emenike, P.A. Sagboye, K.T. Micheal, T. T. Micheal, O.D. Saliu, R. James, Biomass-derived activated carbon monoliths: a review of production routes, performance, and commercialization potential, J. Clean. Prod. 423 (2023) 138711, https://doi.org/10.1016/j.jclepro.2023.138711.

[8] S.H. Dhawane, T. Kumar, G. Halder, Parametric effects and optimization on synthesis of iron (II) doped carbonaceous catalyst for the production of biodiesel, Energy Convers. Manag. 122 (2016) 310–320, https://doi.org/10.1016/j.enconman.2016.06.005.

[9] P. Sahu, S. Gangil, V.K. Bhargav, Biopolymeric transitions under pyrolytic thermal degradation of Pigeon pea stalk, Renew. Energy 206 (2023) 157–167, https://doi.org/10.1016/j.renene.2023.02.012.

[10] S.S. Sahoo, V.K. Vijay, R. Chandra, H. Kumar, Production and characterization of biochar produced from slow pyrolysis of pigeon pea stalk and bamboo, Clean. Eng. Technol. 3 (2021) 100101, https://doi.org/10.1016/j.clet.2021.100101.

[11] N. Kirti, S.P. Tekade, A. Tagade, A.N. Sawarkar, Pyrolysis of pigeon pea (Cajanus cajan) stalk: kinetics and thermodynamic analysis of degradation stages via isoconversional and master plot methods, Bioresour. Technol. 347 (2022) 126440, https://doi.org/10.1016/j.biortech.2021.126440.

[12] R. kumar Singh, A. Sarkar, J.P. Chakraborty, Effect of torrefaction on the physicochemical properties of pigeon pea stalk (Cajanus cajan) and estimation of kinetic parameters, Renew. Energy 138 (2019) 805–819, https://doi.org/10.1016/j.renene.2019.02.022.

[13] E. Ding, J. Jiang, Y. Lan, L. Zhang, C. Gao, K. Jiang, X. Qi, X. Fan, Optimizing Cd2+ adsorption performance of KOH modified biochar adopting response surface methodology, J. Anal. Appl. Pyrolysis 169 (2023) 105788, https://doi.org/10.1016/j.jaap.2022.105788.

[14] A.K. Sakhiya, V.K. Vijay, P. Kaushal, Development of rice straw biochar through pyrolysis to improve drinking water quality in arsenic and manganese contaminated areas, Surf. Interfaces 36 (2023) 102582, https://doi.org/10.1016/j.surfin.2022.102582.

[15] A. Kumar, A. Preetam, K.K. Pant, An integrated eco-friendly and efficient approach towards heavy metal removal from industrial wastewater and co-generating bio-oil using wheat straw via hydrothermal liquefaction, J. Environ. Chem. Eng. 11 (2023) 110217, https://doi.org/10.1016/j.jece.2023.110217.

[16] P. Chakraborty, S. Show, S. Banerjee, G. Halder, Mechanistic insight into sorptive elimination of ibuprofen employing bi-directional AB from sugarcane bagasse: performance evaluation and cost estimation, J. Environ. Chem. Eng. 6 (2018) 5287–5300, https://doi.org/10.1016/j.jece.2018.08.017.

[17] L. Gao, Z. Li, W. Yi, Y. Li, P. Zhang, A. Zhang, L. Wang, Impacts of pyrolysis temperature on lead adsorption by cotton stalk-derived biochar and related mechanisms, J. Environ. Chem. Eng. 9 (2021) 105602, https://doi.org/10.1016/j.jece.2021.105602.

[18] U. Guyo, J. Mhonyera, M. Moyo, Pb(II) adsorption from aqueous solutions by raw and treated biomass of maize stover - a comparative study, Process Saf. Environ. Prot. 93 (2015) 192–200, https://doi.org/10.1016/j.psep.2014.06.009.

[19] A.A. Acosta-Herrera, V. Hernández-Montoya, R. Tovar-Gómez, M. del R. Moreno-Virgen, M.A. Pérez-Cruz, M.Á. Montes-Morán, F.J. Cervantes, Tailored carbon adsorbents developed from coconut shells and coconut palm fibers for the removal of contaminants from anodizing wastewater, J. Mol. Liq. 386 (2023), https://doi.org/10.1016/j.molliq.2023.122471.

[20] F.O. Olanrewaju, G.E. Andrews, H. Li, H.N. Phylaktou, B.G. Mustafa, M.H.M. Kiah, Investigation of the heat release rate and particle generation during fixed bed gasification of sweet sorghum stalk, Fuel 332 (2023), https://doi.org/10.1016/j.fuel.2022.126013.

[21] A. Tagade, S. Kandpal, A.N. Sawarkar, Insights into pyrolysis of pearl millet (Pennisetum glaucum) straw through thermogravimetric analysis: Physico-chemical characterization, kinetics, and reaction mechanism, Bioresour. Technol. 391 (2024) 129930, https://doi.org/10.1016/j.biortech.2023.129930.

[22] L.K.H. Pham, S. Kongparakul, M. Ding, G. Guan, N. Chanlek, P. Reubroycharoen, D. V.N. Vo, N. Van Cuong, C. Samart, High-efficiency catalytic pyrolysis of palm kernel shells over Ni2P/nitrogen-doped activated carbon catalysts, Biomass Bioenergy 174 (2023) 106836, https://doi.org/10.1016/j.biombioe.2023.106836.

[23] N. Maaloul, P. Oulego, M. Rendueles, A. Ghorbal, M. Díaz, Novel biosorbents from almond shells: characterization and adsorption properties modeling for Cu(II) ions from aqueous solutions, J. Environ. Chem. Eng. 5 (2017) 2944–2954, https://doi.org/10.1016/j.jece.2017.05.037.

[24] R. Verma, P.K. Maji, S. Sarkar, Comprehensive investigation of the mechanism for Cr(VI) removal from contaminated water using coconut husk as a biosorbent, J. Clean. Prod. 314 (2021) 128117, https://doi.org/10.1016/j.jclepro.2021.128117.

[25] C. de la Fuente, R. Clemente, I. Martínez-Alcalá, G. Tortosa, M.P. Bernal, Impact of fresh and composted solid olive husk and their water-soluble fractions on soil heavy metal fractionation; microbial biomass and plant uptake, J. Hazard. Mater. 186 (2011) 1283–1289, https://doi.org/10.1016/j.jhazmat.2010.12.004.

[26] V. thi Quyen, T.H. Pham, J. Kim, D.M. Thanh, P.Q. Thang, Q. Van Le, S.H. Jung, T. Y. Kim, Biosorbent derived from coffee husk for efficient removal of toxic heavy metals from wastewater, Chemosphere 284 (2021) 131312, https://doi.org/10.1016/j.chemosphere.2021.131312.

[27] S. Sadaf, H.N. Bhatti, Batch and fixed bed column studies for the removal of Indosol Yellow BG dye by peanut husk, J. Taiwan Inst. Chem. Eng. 45 (2014) 541–553, https://doi.org/10.1016/j.jtice.2013.05.004.

[28] L. Xu, Z. Shu, S. Sun, Y. Wen, J. Zhou, Amorphous Fe–Mn binary oxides nanoparticles decorating waste bamboo biomass-based monolith for efficient arsenic removal with column adsorption, Sep. Purif. Technol. 330 (2024) 125426, https://doi.org/10.1016/j.seppur.2023.125426.

[29] S.L. Narnaware, N.L. Panwar, Kinetic study on pyrolysis of mustard stalk using thermogravimetric analysis, Bioresour. Technol. Rep. 17 (2022) 100942, https://doi.org/10.1016/j.biteb.2021.100942.

[30] M. Aouine, D. Elalami, A. Haggoud, S.I. Koraichi, L. Roumeas, A. Barakat, Dry chemo-mechanical pretreatment of chickpea straw: effect and optimization of experimental parameters to improve hydrolysis yields, Bioresour. Technol. Rep. 18 (2022) 101011, https://doi.org/10.1016/j.biteb.2022.101011.

[31] Z. Du, T. Zheng, P. Wang, L. Hao, Y. Wang, Fast microwave-assisted preparation of a low-cost and recyclable carboxyl modified lignocellulose-biomass jute fiber for enhanced heavy metal removal from water, Bioresour. Technol. 201 (2016) 41–49, https://doi.org/10.1016/j.biortech.2015.11.009.

[32] B. Koul, M. Yakoob, M.P. Shah, Agricultural waste management strategies for environmental sustainability, Environ. Res. 206 (2022) 112285, https://doi.org/10.1016/j.envres.2021.112285.

[33] S.H. Dhawane, A.P. Bora, T. Kumar, G. Halder, Parametric optimization of biodiesel synthesis from rubber seed oil using iron doped carbon catalyst by Taguchi approach, Renew. Energy 105 (2017) 616–624, https://doi.org/10.1016/j.renene.2016.12.096.

[34] S.K. Sahoo, A.K. Purohit, G.K. Panigrahi, J.K. Sahoo, Adsorption of methylene blue from aqueous media using graphene oxide synthesised from bio-soot wastes, Phys. Chem. Liq. 59 (2021) 872–882, https://doi.org/10.1080/00319104.2020.1858418.

[35] S. Alam, B. Ullah, M.S. Khan, N. Ur Rahman, L. Khan, L.A. Shah, I. Zekker, J. Burlakovs, A. Kallistova, N. Pimenov, E. Yandri, R.H. Setyobudi, Y. Jani, M. Zahoor, Adsorption kinetics and isotherm study of basic red 5 on synthesized silica monolith particles, Water (Switzerland) 13 (2021) 1–13, https://doi.org/10.3390/w13202803.

[36] A.M.S. Ngueabouo, R.F.T. Tagne, D.R.T. Tchuifon, C.G. Fotsop, A.K. Tamo, S. G. Anagho, Strategy for optimizing the synthesis and characterization of activated carbons obtained by chemical activation of coffee husk, Mater. Adv. 3 (2022) 8361–8374, https://doi.org/10.1039/d2ma00591c.

[37] S.H. Dhawane, T. Kumar, G. Halder, Biodiesel synthesis from Hevea brasiliensis oil employing carbon supported heterogeneous catalyst: optimization by Taguchi method, Renew. Energy 89 (2016) 506–514, https://doi.org/10.1016/j.renene.2015.12.027.

[38] C. Waghmare, S. Ghodmare, K. Ansari, M.H. Dehghani, M. Amir Khan, M.A. Hasan, S. Islam, N.A. Khan, S. Zahmatkesh, Experimental investigation of H3PO4 activated papaya peels for methylene blue dye removal from aqueous solution: evaluation on optimization, kinetics, isotherm, thermodynamics, and reusability studies, J. Environ. Manag. 345 (2023) 118815, https://doi.org/10.1016/j.jenvman.2023.118815.

[39] P. Barooah, N. Mushahary, B. Das, S. Basumatary, Waste biomass-based graphene oxide decorated with ternary metal oxide (MnO-NiO-ZnO) composite for adsorption of methylene blue dye, clean, Water 2 (2024) 100049, https://doi.org/10.1016/j.clwat.2024.100049.

[40] A.H. Jawad, N.N.A. Malek, T. Khadiran, Z.A. Alothman, Z.M. Yaseen, Mesoporous high-surface-area activated carbon from biomass waste via microwave-assisted-H3PO4 activation for methylene blue dye adsorption: an optimized process, Diam. Relat. Mater. 128 (2022) 109288, https://doi.org/10.1016/j.diamond.2022.109288.

[41] M.C. Kasemodel, L.G. de Aguiar, V.G.S. Rodrigues, É.L. Romão, The investigation of the adsorption of methylene blue from water by torrefied biomass, Colorants 4 (2025) 21, https://doi.org/10.3390/colorants4020021.

[42] A. Fathi, E. Asgari, H. Danafar, H. salehabadi, M.M. Fazli, A comprehensive study on methylene blue removal via polymer and protein nanoparticle adsorbents, Sci. Rep. 14 (2024), https://doi.org/10.1038/s41598-024-80384-4.